Preprints of the 19th World Congress
The International Federation of Automatic Control
Cape Town, South Africa. August 24-29, 2014

Optimal Control of Variable Stiffness Actuators with Nonlinear Springs

Mehmet Can Özparpucu [*] **, Sami Haddadin** [**] **and Alin Albu-Schäffer**[*]

[*] *German Aerospace Center, Institute of Robotics and Mechatronics*
[**] *Institute of Automatic Control (IRT), Leibniz University Hanover*

Abstract: Variable Stiffness Actuators (VSA) are currently being regarded as promising actuator types in robotics research especially due to their capability to store potential energy in their elastic elements and to control this energy by altering the elastic properties of these elements. The controllable potential energy enables these actuators to outperform their rigid counterparts especially when realizing fast explosive motions. Most of joint designs with VSA's, however, are described by nonlinear deflection-torque relations and consequently a thorough analysis regarding their maximum attainable performance is difficult. In this work, we tackle this problem by using Pontryagin's Minimum Principle and develop a general method to solve the optimal control problem of minimizing any given terminal cost for these joints. In other words, we show the optimal control strategies to alter VSA's elastic properties for various tasks such as maximization of the final link velocity or time-optimal tracking, which are all found to depend on the change of the system's potential and kinetic energy relative to its total energy. The application of the method is illustrated for VSA's with adjustable linear and cubic springs, where the potential energy stored in the springs is maximized at a given final time.

1. INTRODUCTION

Inspired by the variable joint stiffness of humans, Variable Stiffness Actuators (VSA) have become a major research field in robotics. Consequently, the number of joint designs with VSA's are increasing vastly (van Ham et al. [2009]). Using compliant elements to connect the links to the motors as done in these designs provides significant advantages. First of all, safer robots can be realized by decoupling the rotor inertia from the links to decrease the impulse a human operator will experience at a collision (Bicchi and Tonietti [2004]). Secondly, decoupling the rotor inertia improves the robustness of these systems, especially in case of unforeseen impacts. Indeed, the impact energy can be absorbed by elastic elements of VSA's and this prevents the system from being damaged in contrast to stiff robots, where impacts mostly lead to failure of these systems particularly when the motor is connected to the link using gear trains (Pratt and Williamson [1995]). A good example for this increased robustness is the DLR Hand Arm System, which is shown to stay undamaged after being hit with a baseball bat (Wolf et al. [2011]). Finally, making use of the stored energy in the elastic elements, the performance of robots with VSA's can significantly be increased. In this paper, we will mainly investigate this last property and try to find the control strategy that maximizes the performance of these actuators.

Numerous works already exist demonstrating the performance gain of joints with VSA's for different motion types, see for ex. Braun et al. [2011], Garabini et al. [2011], Haddadin et al. [2012a,b], Nakanishi and Vijayakumar [2012]. Most of these works use Optimal Control (OC) Theory as a mathematical tool, but they either rely on numerical methods which prevents us from finding a clear physical interpretation of the resulting control strategy or assume simple adjustable linear deflection-torque relations, which is mostly not a valid assumption in real applications. Indeed, for most of the existing joint designs the elastic joint torque in VSA's are represented by adjustable nonlinear functions (Eiberger et al. [2010], Wolf and Hirzinger [2008], Wolf et al. [2011]). In this work, we will focus on this nonlinear deflection-torque relation and make use of Pontryagin's Minimum Principle to discuss how to optimally adjust it to maximize the joint's performance.

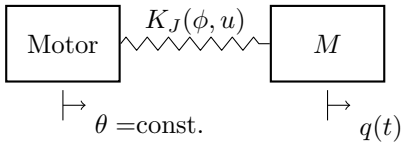

Fig. 1. Joint Model with Variable Stiffness Actuator

The paper is organized as follows. In Section 2, we introduce the joint model with the VSA and define our OC Problem, which consists of only a terminal cost in order to have a control strategy that fully exploits the system dynamics. Section 3 provides necessary conditions for the corresponding OC by applying Pontryagin's Minimum Principle and clarifies the dependence of the control on the system's states and costates. Using these necessary conditions, we then develop in Section 4 a general method to construct the optimal control trajectory, where we describe all the resulting terms using physical quantities to gain a physical understanding. Finally, in order to illustrate how to use the method and also to see how nonlinearities affect the resulting strategy, we investigate the OC strategy to maximize the potential energy in two different VSA's consisting of adjustable linear and cubic springs, respectively.

2. PROBLEM FORMULATION

In this paper, we investigate elastic joints consisting of one link, one fixed motor and finally a VSA that connects the link to the motor, see Figure 1. The joint torque τ_J in the spring, which acts on both the motor and link, depends not only on the angular deflection ϕ but also on the torque profile that can vary due to VSA. We let the elastic joint torque τ_J to be directly controlled such that it is constrained between two continuously differentiable functions of the angular deflection $\tau_{J,1}, \tau_{J,2}$ with

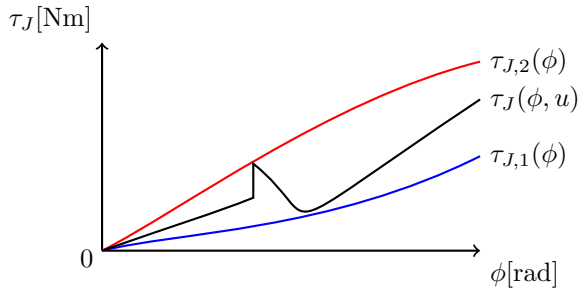

Fig. 2. Controllable Elastic Joint Torque in the VSA

$$\tau_J(\phi,u)=\frac{1}{2}\left(\tau_{J,2}(\phi)+\tau_{J,1}(\phi)\right)+\frac{u}{2}\left(\tau_{J,2}(\phi)-\tau_{J,1}(\phi)\right), \tag{1}$$

where $\tau_{J,1}<\tau_{J,2}$ holds for all $\phi>0$ and $u\in[-1,1]$ denotes the piecewise continuous control. The two functions $\tau_{J,1}$ and $\tau_{J,2}$ will furthermore be assumed to be strictly increasing and symmetrical with respect to the origin. Figure 2 visualises one possible choice for $\tau_{J,1}$,$\tau_{J,2}$ and the controlled torque $\tau_J(\phi,u)$. The dynamics of the joint model illustrated in Fig. 1 can simply be described using Newton's second law with equation (1) as:

$$M\ddot{q}=\tau_J(\phi,u), \tag{2}$$

where $M>0$ stands for the link's mass of intertia, q for the link position, $\theta=$ const. for the fixed motor position, $\phi=\theta-q$ for the angular deflection and finally u for the control of VSA as already mentioned. Without loss of generalization, we let the motor position $\theta=0$ and obtain the following first-order differential equations which we need to apply Pontryagin's Minimum Principle (Papageorgiou [1996]):

$$\boldsymbol{f}(u,\boldsymbol{x}):=\dot{\boldsymbol{x}}=\begin{pmatrix}\dot{\phi}\\ \ddot{q}\end{pmatrix}=\begin{pmatrix}-\dot{q}\\ \dfrac{\tau_J(\phi,u)}{M}\end{pmatrix}=\begin{pmatrix}-x_2\\ \dfrac{\tau_J(x_1,u)}{M}\end{pmatrix}, \tag{3}$$

where the state is given by $\boldsymbol{x}=(\phi\ \dot{q})^T$. Note that, with this particular choice of the states, we can easily investigate the change of the potential energy as well as the kinetic energy by merely looking at the evolution of the states, since both are closely related. This property will be useful when we later describe the optimal control strategy in terms of physical quantities.

In order to fully define an OC problem, we need to choose a cost functional, which is to be minimized by the optimal control. As already mentioned, we want to find control strategies that fully exploit the system dynamics. In other words, we do not necessarily consider the way a final state is reached. Consequently, we omit any running costs and deal in this paper with cost functionals consisting of only a terminal cost:

$$J(u)=\vartheta(\boldsymbol{x}(t_f),t_f), \tag{4}$$

where the terminal cost $\vartheta(\boldsymbol{x}(t_f),t_f)$ can be chosen according to the investigated performance criterion. As we will see, all the optimal controls minimizing a given terminal cost need to satisfy similar necessary conditions, which is why at this step we do not specify ϑ in more detail. In the following section, we will make use of Pontryagin's Minimum Principle to derive these necessary conditions.

3. NECESSARY CONDITIONS

In order to apply Pontryagin's Minimum Principle, we need to first build the Hamiltonian $\mathbb{H}$, which depends on the system dynamics and the cost functional. For the given system (3) and the cost functional (4) the Hamiltonian becomes (Papageorgiou [1996]):

$$\mathbb{H}=\boldsymbol{\lambda}^T\boldsymbol{f}=-\lambda_1x_2+\lambda_2\frac{\tau_J(x_1,u)}{M}, \tag{5}$$

with $\boldsymbol{\lambda}$ denoting the costates of the system. This particular Hamiltonian $\mathbb{H}$ is known to be minimized by the optimal control u^* along the optimal trajectory $\boldsymbol{x}^*$ and $\boldsymbol{\lambda}^*$, so that we have:

$$\mathbb{H}(\boldsymbol{x}^*,\boldsymbol{\lambda}^*,u^*)\leq\mathbb{H}(\boldsymbol{x}^*,\boldsymbol{\lambda}^*,u), \tag{6}$$

for all $u\in[-1,1]$. Evaluating this inequality for the Hamiltonian in (5) and using the torque relation for the VSA in (1) we have:

$$\lambda_2^*\left[\tau_{J,2}(x_1^*)-\tau_{J,1}(x_1^*)\right]u^*\leq\lambda_2^*\left[\tau_{J,2}(x_1^*)-\tau_{J,1}(x_1^*)\right]u. \tag{7}$$

According to the assumptions we had for $\tau_{J,1}$ and $\tau_{J,2}$, we have then the following relations for u^*:

$$u^*=\begin{cases}-1 & x_1^*\lambda_2^*>0\\ 1 & x_1^*\lambda_2^*<0\\ \text{singular} & x_1^*\lambda_2^*=0\end{cases}. \tag{8}$$

The trajectory of the optimal angular deflection x_1^* and the optimal second costate λ_2^* play thus a significant role in determining the optimal torque profile. According to Minimum Principle, the partial derivatives of the Hamiltonian with respect to $\boldsymbol{x}$ provide the system dynamics of the costates (Papageorgiou [1996]):

$$\dot{\boldsymbol{\lambda}}=-\frac{\partial\mathbb{H}}{\partial\boldsymbol{x}}=\begin{pmatrix}-\dfrac{\partial\tau_J(x_1,u)}{\partial x_1}\dfrac{\lambda_2}{M}\\ \lambda_1\end{pmatrix}. \tag{9}$$

In order to better understand the trajectory of the costates, it is instructive to find a mechanical analog for this particular set of first-order differential equations. Differentiating the second row of (9) with respect to time and using its first row, we can first obtain:

$$M\ddot{\lambda}_2+\frac{\partial\tau_J(x_1,u)}{\partial x_1}\lambda_2=0. \tag{10}$$

Since $\frac{\partial\tau_J(x_1,u)}{\partial x_1}=(\frac{1+u}{2})\frac{\mathrm{d}\tau_{J,2}}{\mathrm{d}x_1}+(\frac{1-u}{2})\frac{\mathrm{d}\tau_{J,1}}{\mathrm{d}x_1}\geq0$ holds for the strictly increasing functions $\tau_{J,1}$ and $\tau_{J,2}$ when $u\in[-1,1]$, we can conclude that equation (10) describes an elastic joint with a spring similar to the joint depicted in Figure 1. Furthermore, the stiffness of this new joint corresponds to the instantaneous stiffness $\frac{\partial\tau_J(\phi,u)}{\partial\phi}$ of the original joint described by (2). We will make more use of equation (10), as we derive analytical expressions for the costates. According to the necessary conditions (8), which need to be satisfied by the optimal control u^*, Minimum Principle does not give any information regarding the optimal control strategy, if a singularity occurs. In order to better understand when such a singularity can occur, we turn our focus now to the singularity of u^* and provide conditions under which singular arcs can be ignored.

3.1 Singularity of the Optimal Control

The control u^* will only be singular if $x_1^*\lambda_2^*=0$ holds in a finite time interval $t\in[t_s,t_s+\varepsilon]$ with $\varepsilon>0$. In order for this product to remain at zero, $x_1^*=0$ or $\lambda_2^*=0$ must hold in a finite time interval. We focus now on these two possibilities.

If $x_1^*=0$, then $\dot{x}_1^*=-x_2^*=0$ holds, as well. In this case, $\boldsymbol{x}^*$ is identically zero and the controls can not change the system's state since $\tau_J(0,u)=0$ holds for any u. In other words, $\boldsymbol{x}=\boldsymbol{0}$ is an isolated point of the system (3) and there is nothing to solve. Similar to the angular deflection

x_1^*, λ_2^* can only stay at zero, if $\dot{\lambda}_2^* = \lambda_1^* = 0$ holds. Since $\boldsymbol{\lambda} = \mathbf{0}$ is an isolated point for the costates as well, $\boldsymbol{\lambda}^*$ will then be identically zero.

The OC problems, which we will deal with in this paper, will be restricted to those for which both $\boldsymbol{x}^*$ and $\boldsymbol{\lambda}^*$ are not identically zero. Note that in the presence of this restriction, we can still derive the optimal control strategy in most cases, as Minimum Principle provides in general non-zero boundary conditions of the costates at the final time as follows (Papageorgiou [1996]):

$$\left(\frac{\delta\vartheta}{\delta\boldsymbol{x}}\Big|_{t_f,\boldsymbol{x}_f^*} + \frac{\delta\boldsymbol{g}}{\delta\boldsymbol{x}}\Big|_{t_f,\boldsymbol{x}_f^*}\boldsymbol{\nu}^* - \boldsymbol{\lambda}^*(t_f)\right)^T \delta\boldsymbol{x}_f = 0, \quad (11)$$

where $\boldsymbol{g}(\boldsymbol{x}^*(t_f), t_f) = \mathbf{0} \in \mathbb{R}^l$ denotes any given end constraints and $\boldsymbol{\nu}^* \in \mathbb{R}^l$ a constant vector. For instance, we have for the OC problem of maximizing the angular deflection

$$J = -x_1(t_f) \overset{(11)}{\Rightarrow} \boldsymbol{\lambda}^*(t_f) = \frac{\delta\vartheta}{\delta\boldsymbol{x}}\Big|_{t_f,\boldsymbol{x}_f^*} = \begin{pmatrix}-1\\0\end{pmatrix} \neq \mathbf{0}, \quad (12)$$

and our restriction is not violated. Once we derive the equations needed to obtain the OC strategy, we will investigate this particular OC problem for VSA's with linear and cubic torque profiles in detail (see Sec. 4.4).

To sum up, for OC problems where $\boldsymbol{x}^*$ and $\boldsymbol{\lambda}^*$ are not identically zero, we now know that the optimal control u^* will always take its minimum or maximum value along the optimal trajectory. According to (8) we can then write for the optimal control u^*:

$$u^* = -\mathrm{sgn}(\lambda_2^* x_1^*). \quad (13)$$

In the following section, we will make use of this bang-bang property of the optimal control to derive the equations that will yield the optimal trajectory.

4. CONSTRUCTING THE OPTIMAL TRAJECTORY

Since we constrain ourselves to OC problems with nonzero $\boldsymbol{x}$ and $\boldsymbol{\lambda}$, we know from the previous section, that u^* is bang-bang. The optimal deflection-torque relation will then switch between $\tau_{J,1}(\phi)$ and $\tau_{J,2}(\phi)$. For a constant control $u^* \in \{-1, 1\}$, the dynamics of the angular deflection can be rewritten similar to (2) [1]:

$$M\ddot{x}_1 + \tau_{J,i}(x_1) = 0, \quad (14)$$

where $i \in \{1, 2\}$ and $\tau_{J,1}$ is obtained when $u^* = -1$ and $\tau_{J,2}$ when $u^* = 1$. It is important to note that both x_1 and $\dot{x}_1 = -x_2$ are continuous and that equation (14) describes a conservative system with the total energy:

$$E = \frac{1}{2}M\dot{x}_1^2 + \int_0^{x_1} \tau_{J,i}(\xi)\mathrm{d}\xi. \quad (15)$$

Furthermore, as long as E remains constant, both the angular displacement x_1 and its time derivative $\dot{x}_1$ will oscillate with a certain period. This period will in general not only depend on $\tau_{J,i}$ but also on the Enegy E, unless the spring is linear (Nayfeh and Mook [1995]).

Since E is constant, we can make use of equation (15) to express the velocity $\dot{x}_1$ in terms of the angular deflection:

$$\dot{x}_1(x_1) = \pm\sqrt{\frac{2(E - \int_0^{x_1}\tau_{J,i}(\xi)\mathrm{d}\xi)}{M}}. \quad (16)$$

Note that for constant enery E, the maximum velocity will be obtained whenever the angular deflection x_1 is zero. We will denote this velocity with $\dot{\phi}_{max} := \dot{x}_1(x_1 = 0)$. Furthermore, the sign of the system's angular velocity $\dot{x}_1$ changes at the maximal deflections $x_1 = \pm\phi_{max}$, where the energy E is fully stored in the spring:

$$E \overset{!}{=} \int_0^{\phi_{max}} \tau_{J,i}(\xi)\mathrm{d}\xi. \quad (17)$$

Since the optimal control u^* depends on the angular deflection (see (8)), one might try to use (16), to derive a relation between the deflection x_1 and the current time t by integration:

$$\pm\int_{x_1(t_0)}^{x_1(t)} \sqrt{\frac{M}{2(E - \int_0^{x_1}\tau_{J,i}(\xi)\mathrm{d}\xi)}}\mathrm{d}x_1 = t - t_0. \quad (18)$$

The integral in (18) can usually not be written in closed-form and this complicates finding an expression for the angular deflection x_1 as a function of time t. Furthermore, for nonlinear springs the deflection $x_1(t)$ influences the dynamics of the costates $\boldsymbol{\lambda}$, since the instantaneous stiffness in (10) depends on the current angular displacement. It is thus not straightforward to solve the differential equations corresponding to the costates, if $\boldsymbol{\lambda}$ is to be expressed as a function of time. For that reason, we follow another approach and search for an expression of the costates in terms of the angular deflection. In particular, we want to see how the OC strategy is related to the potential energy stored in the spring, which is known to determine the OC strategy for variable stiffness joints with linear springs (Haddadin et al. [2012b]). In order to show this relation, we will follow four main steps: We will first derive second order differential equations for λ_2 along the trajectory of the angular deflection and discuss its solution, which we express in terms of physical quantities. The resulting differential equations will have singularities, which will be discussed in the second step. Using the derived expression for λ_2 together with the relation (13), the switching structure of u^* will be derived, where we also investigate the influence of a switch in the control on the optimal trajectory. Finally, it will be shown how the obtained results can be used to solve the OC problem of maximizing the potential energy of elastic joints with two different VSA's.

4.1 Differential Equation and Solution for $\lambda_2(x_1)$

In the following, we will find a description of the second costate λ_2 in terms of the angular deflection x_1 by making use of the differential equation (10). Note that this equation describes the dynamics of λ_2 in terms of its time derivatives, whereas we want to investigate the change of λ_2 along the angular displacement x_1. In order to make use of (10), we need to first rewrite this equation such that it only contains the costate's derivatives with respect to x_1. Applying the chain rule (Rudin [1976]) to the time derivatives of $\lambda_2(x_1)$, we have:

$$\dot{\lambda}_2 = \frac{\mathrm{d}\lambda_2}{\mathrm{d}x_1}\frac{\mathrm{d}x_1}{\mathrm{d}t} = \frac{\mathrm{d}\lambda_2}{\mathrm{d}x_1}\dot{x}_1 \quad (19)$$

$$\ddot{\lambda}_2 = \frac{\mathrm{d}}{\mathrm{d}t}(\frac{\mathrm{d}\lambda_2}{\mathrm{d}x_1}\dot{x}_1) = \frac{\mathrm{d}^2\lambda_2}{\mathrm{d}x_1^2}\dot{x}_1^2 + \frac{\mathrm{d}\lambda_2}{\mathrm{d}x_1}\ddot{x}_1. \quad (20)$$

Note that the two derivatives $\frac{\mathrm{d}\lambda_2}{\mathrm{d}x_1}$ and $\frac{\mathrm{d}^2\lambda_2}{\mathrm{d}x_1^2}$ in (19)-(20) are well-defined, unless $\dot{x}_1 = 0$ or equivalently $x_1 = \pm\phi_{max}$. Furthermore, both λ_2 and $\dot{\lambda}_2 = \lambda_1$ are continuous according to Minimum Principle. In addition, since $\frac{\mathrm{d}\tau_{J,i}(x_1)}{\mathrm{d}x_1}$ is continuous from our initial assumption, $\ddot{\lambda}_2$ is continuous as well (see (10)). Consequently, we can conclude that both $\frac{\mathrm{d}\lambda_2}{\mathrm{d}x_1}$ and $\frac{\mathrm{d}^2\lambda_2}{\mathrm{d}x_1^2}$ are continuous in $x_1 \in (-\phi_{max}, \phi_{max})$. We can now substitute the time derivatives of λ_2 in equation

[1] Take the time derivative of the first row of (3) and use its second row to obtain this relation.

(10) with its derivatives with respect to x_1 using (19)-(20). This leads to the following linear differential equations:

$$M\dot{x}_1^2\frac{\mathrm{d}^2\lambda_2}{\mathrm{d}x_1^2} + M\ddot{x}_1\frac{\mathrm{d}\lambda_2}{\mathrm{d}x_1} + \frac{\mathrm{d}\tau_{J,i}}{\mathrm{d}x_1}\lambda_2 = 0 \tag{21}$$

$$\Rightarrow \frac{\mathrm{d}}{\mathrm{d}x_1}\left(\dot{x}_1^2(x_1)\frac{\mathrm{d}\lambda_2}{\mathrm{d}x_1} + \frac{\tau_{J,i}(x_1)}{M}\lambda_2\right) = 0, \tag{22}$$

where we make use of the relation $\frac{\mathrm{d}}{\mathrm{d}x_1}\dot{x}_1^2(x_1) = -2\frac{\tau_{J,i}(x_1)}{M} = 2\ddot{x}_1$ (see (14) and (16)). Note that the last equation (22) is a linear first-order differential equation with singularities at $x_1 = \pm\phi_{max}$. Its analytical solution can simply be found using variation of constants (Braun [1993]) as:

$$\lambda_2(x_1) = \left|\frac{\dot{x}_1(x_1)}{\dot{\phi}_{max}}\right|\left(\lambda_2(0) + \frac{\mathrm{d}\lambda_2}{\mathrm{d}x_1}(0)\int_0^{x_1}\left|\frac{\dot{x}_1(\xi)}{\dot{\phi}_{max}}\right|^{-3}\mathrm{d}\xi\right). \tag{23}$$

This solution for $\lambda_2(x_1)$ is uniquely determined in $x_1 \in (-\phi_{max}, \phi_{max})$ by the boundary conditions $\lambda_2(0)$ and $\frac{\mathrm{d}\lambda_2}{\mathrm{d}x_1}(0)$, which are evaluated at $x_1 = 0$. In addition, at the singularities $x_1 = \pm\phi_{max}$, λ_2 will take the value $\lim_{x_1\to\pm\phi_{max}}\lambda_2(x_1) = \frac{\mathrm{d}\lambda_2}{\mathrm{d}x_1}(0)\frac{M\dot{\phi}_{max}^2}{\tau_{J,i}(\pm\phi_{max})}$. Using (22), we can now find an analytical solution for the derivative $\frac{\mathrm{d}\lambda_2}{\mathrm{d}x_1}$:

$$\frac{\mathrm{d}\lambda_2}{\mathrm{d}x_1} = \frac{1}{\dot{x}_1^2(x_1)}\left(\dot{\phi}_{max}^2\frac{\mathrm{d}\lambda_2}{\mathrm{d}x_1}(0) - \frac{\tau_{J,i}(x_1)}{M}\lambda_2(x_1)\right), \tag{24}$$

which is however not defined at the singularities as already expected from (19). The two analytical expressions (23)-(24) play a significant role for understanding the optimal trajectory, since they describe the costates on which the optimal strategy depends in terms physical quantities. For instance, we see from (23) that λ_2 merely depends on the ratio $\left|\frac{\dot{\phi}}{\dot{\phi}_{max}}\right|$, which indicates how much of the system's energy is converted into the link's kinetic energy. According to (24), not only this ratio but also the acceleration $\ddot{x}_1 = -\frac{\tau_{J,i}(x_1)}{M}$ has an effect on the value of $\frac{\mathrm{d}\lambda_2}{\mathrm{d}x_1}$.

In order to simplify the illustration of the costates graphically and also have a better understanding of the potential energy change relative to the total energy, we introduce here the normalized angular deflection $\bar{x}_1$ defined as:

$$\bar{x}_1 = \frac{x_1}{\phi_{max}}. \tag{25}$$

Similar to the ratio $\left|\frac{\dot{\phi}}{\dot{\phi}_{max}}\right|$, this normalized angular deflection indicates the percentage of the total energy that is stored in the springs as potential energy. Note that with this notation $\bar{x}_1 \in [-1, 1]$ holds and consequently, the singularities of the differential equation will occur at $\bar{x}_1 = \pm 1$. Corresponding to this normalized deflection $\bar{x}_1$, we also define a new derivative λ_2' defined as $\lambda_2' := \frac{\mathrm{d}\lambda_2}{\mathrm{d}\bar{x}_1} = \frac{1}{\phi_{max}}\frac{\mathrm{d}\lambda_2}{\mathrm{d}x_1}$. Using these two additional variables, equation (23) becomes:

$$\lambda_2(\bar{x}_1) = \left|\frac{\dot{x}_1(\bar{x}_1)}{\dot{\phi}_{max}}\right|\left(\lambda_{20} + \lambda_{20}'I(\bar{x}_1)\right), \tag{26}$$

where $\lambda_{20} := \lambda_2(\bar{x}_1 = 0)$, $\lambda_{20}' := \lambda_2'(\bar{x}_1 = 0)$ and $I(\bar{x}_1) := \int_0^{\bar{x}_1}\left|\frac{\dot{x}_1(\xi)}{\dot{\phi}_{max}}\right|^{-3}\mathrm{d}\xi$. Figure 3 depicts the response of the two systems (10) and (14) for a cubic joint torque ($u =$ const.) described by $\tau_J(\phi) = k_c\phi^3$, where the response is computed numerically using adaptive Gauss-Kronrod quadrature (Shampine [2008]) ($M = 1\mathrm{kg}m^2$,$k_c = 2\frac{Nm}{rad^3}$, $x_1(0) = 0$, $\dot{x}_1(0) = 2\frac{rad}{s}$, $\lambda_2(0) = 2$, $\dot{\lambda}_2(0) = 4\frac{1}{s}$).

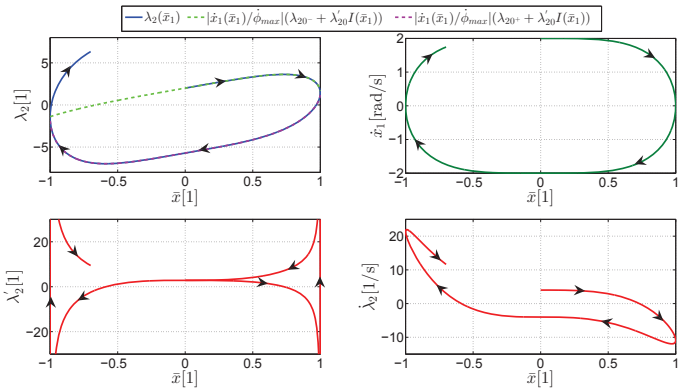

Fig. 3. $\boldsymbol{\lambda}(\bar{x}_1)$ and $\dot{x}_1(\bar{x}_1)$ for a Cubic Stiffness Profile

According to Fig. 3, the value of λ_2' at $\bar{x}_1 = 0$ stays at the same value, whereas λ_2 takes different values at this position. In other words, the boundary condition λ_{20} changes its value along the optimal trajectory unlike λ_{20}'. In Fig. 3 the first two values for λ_{20} are denoted by λ_{20^-} and λ_{20^+}. It is important to note that this change in λ_{20} can only occur at the singularities $\bar{x}_1 = \pm 1$, since the solution (26) uniquely determines $\lambda_2(\bar{x}_1)$ between the singularities $\bar{x}_1 \in (-1, 1)$. In order to fully describe the costate trajectory we need to be able to compute the change in λ_{20}. For that reason, we turn our attention in the following section to the behaviour of λ_2 and λ_2' at the singularities.

4.2 Singularities of the Differential Equation ($\bar{x}_1 = \pm 1$)

According to Minimum Principle, the costates $\lambda_1 = \dot{\lambda}_2$ and λ_2 are continuous at every point of the optimal trajectory. Consequently, they are continuous at the singularities $\bar{x}_1$ as well. We will make use of this continuity at the singularities, to see whether the boundary conditions λ_{20} and λ_{20}' change. Similar to the notation used in Figure 3, we denote the trajectory of the costates before it reaches the singularity with $\lambda_{2^-}, \lambda_{2^-}'$ and afterwards with $\lambda_{2^+}, \lambda_{2^+}'$. Since λ_2 is continuous, we have at $\bar{x}_1 = \pm 1$:

$$\begin{aligned}\lambda_{2^-}(\pm 1) &= \lambda_{2^+}(\pm 1)\\ \overset{(26)}{\Rightarrow}\ \frac{M\dot{\phi}_{max}^2\lambda_{20^-}'}{\tau_{J,i}(\pm\phi_{max})\phi_{max}} &= \frac{M\dot{\phi}_{max}^2\lambda_{20^+}'}{\tau_{J,i}(\pm\phi_{max})\phi_{max}}\\ \Leftrightarrow \lambda_{20^-}' &= \lambda_{20^+}'.\end{aligned} \tag{27}$$

We already observed the equality (27) in Figure 3, where we saw that λ_2' always takes the same value at $\bar{x}_1 = 0$. In this same Figure, we also observed that λ_2 can take different values at $\bar{x}_1 = 0$. This change in λ_{20} can be computed using the continuity of $\dot{\lambda}_2 = \dot{x}_1\frac{\mathrm{d}\lambda_2}{\mathrm{d}x_1}$. Using the analytical solution for $\frac{\mathrm{d}\lambda_2}{\mathrm{d}x_1}$ in (24) with (16), (17), (19) and (26) we first obtain the following expression:

$$\dot{\lambda}_2(\bar{x}_1) = -\frac{\tau_{J,i}(x_1)}{M\dot{\phi}_{max}}\mathrm{sgn}(\dot{x}_1)\left(\lambda_{20} + C(\bar{x}_1)\lambda_{20}'\right), \tag{28}$$

where $C(\bar{x}_1) := I(\bar{x}_1) - \frac{M\dot{\phi}_{max}^3}{\tau_{J,i}(x_1)\phi_{max}|\dot{x}_1(\bar{x}_1)|}$ is a function that is symmetrical with respect to the origin. Note that equation (28) depends on the sign of $\dot{x}_1$. Consequently, if both boundary conditions λ_{20} and λ_{20}' would have stayed constant, $\dot{\lambda}_2$ would in general have a jump at the singularities $\bar{x}_1 = \pm 1$, which is a contradiction. We have already shown that λ_{20}' does not change and thus we can

conclude that λ_{20} must jump when $\dot{\lambda}_2(\pm 1) = 0$. Evaluating (28) at $\bar{x}_1 = \pm 1$, we can conclude:

$$\lambda_{20^+} = -\lambda_{20^-} \pm \Delta \cdot \lambda_{20}^{'}, \tag{29}$$

where $\Delta := 2 \lim_{\bar{x}_1 \to 1^-} C(\bar{x}_1)$. This particular constant is to be subtracted from λ_{20^-} after the positive singularity $\bar{x}_1 = 1$ is reached and added if the negative singularity $\bar{x}_1 = -1$ is reached.

The four equations (26)-(29) can now be used to construct the costates assuming the control u stays constant. Table 1 summarizes some of these analytical expressions for different torque profiles [2]. Using the analytical expressions we derived for the costates, we will next discuss the switching structure for the optimal control along the optimal trajectory.

4.3 Switching Structure

Since the optimal control is bang-bang, the optimal control u^* is uniquely determined by the switching positions, at which it changes its sign. According to (13), the switching structure for u^* can be obtained by investigating the sign of the product $x_1^* \lambda_2^*(x_1^*)$ along the optimal trajectory. Using the analytical expression for $\lambda_2(\bar{x}_1)$ in (26), we can then conclude that the switching positions will depend on the boundary conditions λ_{20} and $\lambda_{20}^{'}$. Remember that in our discussions in the two previous Sections 4.1-4.2 we assumed that u remains at a constant value. However, determining the switching positions for a constant control is not sufficient to determine the switching structure along the whole optimal trajectory. We also need to find how a change in the control influences the states and costates.

In the following two subsections, we first show the dependence of the switching positions on the boundary conditions, and provide a graphical illustration that depicts the optimal control u^* along the optimal trajectory. Then, we discuss the influence of a switching in u^* on the states and costates. Combining the two results will yield the optimal switching structure.

Switching Positions $\bar{x}_1^*$ and the Control u^* As already mentioned the switching positions of the control u^*, which we will denote with $\bar{x}_1^*$, can simply be computed by determining the positions, where the product $x_1^* \lambda_2^*$ changes its sign. Since both x_1^* and λ_2^* are continuous, the first obvious candidate for the switching position is $\bar{x}_1^* = 0$. According to (13), if λ_2^* does not change its sign when the link passes through its equilibrium position $x_1 = 0$, the control u^* will switch. Other candidates for the switching positions are then the positions at which $\lambda_2^*(\bar{x}_1^*)$ is zero. In order to fully construct the optimal trajectory, we have to also find these non-zero states $\bar{x}_1^*$ at which λ_2^* equals to zero. Equation (26) provides the dependence of λ_2 on the position $\bar{x}_1$, which we need to compute these states. Using (26) we can conclude that if $\lambda_{20}^{'} = 0$, λ_2 will be equal to zero at the singularities $\bar{x}_1^* = \pm 1$, whereas if $\lambda_{20}^{'} \neq 0$ at $\bar{x}_1^*$ satisfying

$$I(\bar{x}_1^*) = \int_0^{\bar{x}_1^*} \left| \frac{\dot{x}_1(\xi)}{\dot{\phi}_{max}} \right|^{-3} \mathrm{d}\xi \stackrel{!}{=} -\frac{\lambda_{20}}{\lambda_{20}^{'}}. \tag{30}$$

[2] The function $F(a;b) := \int_0^a \frac{\mathrm{d}\xi}{(1-\xi^2)(1-b^2\xi^2)}$ stands for the incomplete elliptic integral of the first kind, $\tilde{F}(a,b;c;z) := \sum_{i=0}^{\infty} \frac{(a)_s (b)_s}{(c)_s s!} z^s = 1 + \frac{ab}{c} z + \frac{a(a+1)b(b+1)}{c(c+1)2!} z^2 + \dots$ for the hypergeometric function and finally $\Gamma(a) := \int_0^{\infty} t^{a-1} e^t \mathrm{d}t$ for the gamma function (Abramowitz and Stegun [1964]). The constant $j := \sqrt{-1}$ is used to denote the unit imaginary number.

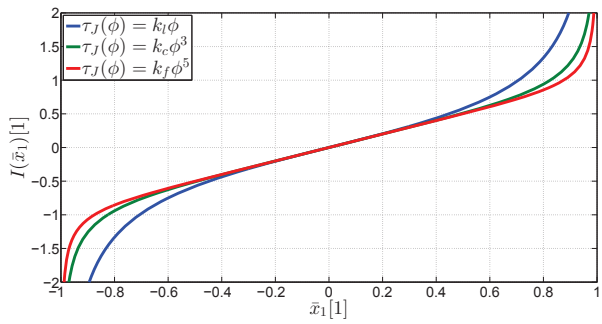

Fig. 4. The Integral $I(\bar{x}_1)$

Note that for a constant control u, the ratio $r := \frac{\lambda_{20}}{\lambda_{20}^{'}}$ stays constant along the trajectory, unless a singularity $\bar{x}_1 = \pm 1$ is reached. In addition, the change of this ratio at these singularities can be computed using (27) and (29). To better comprehend the possible switching positions $\bar{x}_1^*$ with $\lambda_2^*(\bar{x}_1^*) = 0$, we take now a closer look at the integral $I(\bar{x}_1)$ in (30).

Figure 4 depicts the integral $I(\bar{x}_1)$ corresponding to three different torque profiles, for which analytical expressions are provided in Table 1. As seen in the figure, $I(\bar{x}_1)$ is always symmetrical with respect to the origin, since $I(-\bar{x}_1) = -I(\bar{x}_1)$ holds for the symmetric function $\tau_J(\phi)$ (see (16) and (30)). In addition, $I(\bar{x}_1)$ is monotonically increasing in $\bar{x}_1 \in (-1,1)$, since $\frac{\mathrm{d}I}{\mathrm{d}\bar{x}_1} = \left| \frac{\dot{x}_1(\bar{x}_1)}{\dot{\phi}_{max}} \right|^{-3} > 0$ holds in this interval. Finally, the integral $I(\bar{x}_1)$ always tends to infinity at the singular points $\bar{x}_1 = \pm 1$, regardless of the torque profile (see Appendix A). In order to find the switching positions $\bar{x}_1^*$ at which λ_2^* equals to zero, we can now make use of Figure 4, by investigating the intersection points of $-I(\bar{x}_1)$ with the ratio $r = \frac{\lambda_{20}}{\lambda_{20}^{'}}$ (see (30)). Figure 4 indicates thus the dependence of the switching positions on the boundary conditions λ_{20} and $\lambda_{20}^{'}$. The integral $I(\bar{x}_1)$ in Figure 4 can also be used to determine the sign of u^* along the optimal trajectory. Using (13) and (26), we can indeed see how u^* depends on the ratio r:

$$u^* = \begin{cases} -\mathrm{sgn}\left(\bar{x}_1 \lambda_{20}^{'} \left[I(\bar{x}_1) + r\right]\right), & \lambda_{20}^{'} \neq 0 \\ -\mathrm{sgn}\left(\bar{x}_1 \lambda_{20}\right), & \lambda_{20}^{'} = 0 \end{cases}. \tag{31}$$

This last equation shows how the optimal control depends on the two boundary conditions, λ_{20} and $\lambda_{20}^{'}$ with the corresponding ratio r, on the integral $I(\bar{x}_1)$ and finally on the normalized displacement $\bar{x}_1$. A graphical representation of the equation is given in Figure 5 along with the corresponding optimal joint torque profiles $\tau_{J,1}$ and $\tau_{J,2}$. Note that using Figure 5 and the way the phase plots are divided, we can also see that, once the intersection point $r = -I(\bar{x}_1^*) \neq 0$ is reached, the control has to switch, since the link velocity will not change its sign in $\bar{x}_1 \in (-1,1)$. Furthermore, if $\lambda_{20}^{'} = 0$, the control will always switch at the singularities or equivalently at the maximum deflections, since λ_{20} changes its sign at $\bar{x}_1^* = \pm 1$ (see (29)).

Having found the dependence of the switching positions and the optimal control in terms of the ratio $r = \frac{\lambda_{20}}{\lambda_{20}^{'}}$, we focus now on how the boundary conditions λ_{20} and $\lambda_{20}^{'}$ change with a switching of the control u^*.

$\tau_J(\phi)$	$k_l\phi$	$k_c\phi^3$	$k_f\phi^5$
E	$\frac{1}{2}M\dot{x}_1^2+\frac{1}{2}kx_1^2 \stackrel{!}{=} \frac{1}{2}k_l\phi_{max}^2$	$\frac{1}{2}M\dot{x}_1^2+\frac{1}{4}k_cx_1^4 \stackrel{!}{=} \frac{1}{4}k_c\phi_{max}^4$	$\frac{1}{2}M\dot{x}_1^2+\frac{1}{6}k_fx_1^6 \stackrel{!}{=} \frac{1}{6}k_f\phi_{max}^6$
$I(\bar{x}_1)$	$\frac{\bar{x}_1}{\sqrt{1-\bar{x}_1^2}}$	$\frac{1}{2}\left(\frac{\bar{x}_1}{\sqrt{1-\bar{x}_1^4}}+F(\bar{x}_1;j)\right)$	$\bar{x}_1\frac{\tilde{F}(1,-\frac{1}{3};\frac{7}{6};\bar{x}_1^6)}{\sqrt{1-\bar{x}_1^6}}$
$\lambda_2(\bar{x}_1)$	$\sqrt{1-\bar{x}_1^2}\lambda_{20}+\bar{x}_1\lambda_{20}^{'}$	$\sqrt{1-\bar{x}_1^4}\lambda_{20}+\frac{1}{2}\left(\bar{x}_1+\sqrt{1-\bar{x}_1^4}F(\bar{x}_1;j)\right)\lambda_{20}^{'}$	$\sqrt{1-\bar{x}_1^6}\lambda_{20}+\bar{x}_1\tilde{F}(1,-\frac{1}{3};\frac{7}{6};\bar{x}_1^6)\lambda_{20}^{'}$
$C(\bar{x}_1)$	$-\frac{\sqrt{(1-\bar{x}_1^2)}}{\bar{x}_1}$	$\frac{1}{2\bar{x}_1^3}\left(F(\bar{x}_1,j)-\sqrt{1-\bar{x}_1^4}\right)$	$\frac{1}{3\bar{x}_1^5}\left(\frac{3\bar{x}_1^6\tilde{F}(1,-\frac{1}{3};\frac{7}{6};\bar{x}_1^6)-1}{\sqrt{1-\bar{x}_1^6}}\right)$
Δ	0	$F(1,j)$	$\frac{\sqrt{3}\pi^2}{27}2^{\frac{8}{3}}\Gamma(\frac{2}{3})^{-3}$

Table 1. Analytical Expressions for different Torque Profiles

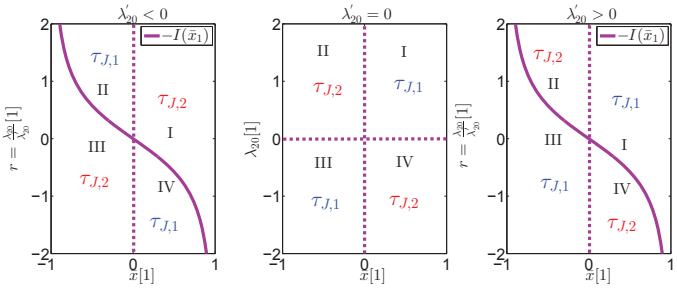

Fig. 5. Optimal Torques along the Optimal Trajectory

Behaviour at the Switchings We have just shown how to determine the positions $\bar{x}_1^*$, at which the control and thus the torque profile changes. When the control switches at these positions an instantaneous change in the torque profile occurs, which in general changes the potential energy stored in the spring. The amount of this instantaneous energy change depends on the adjustable torque profiles and the particular switching position. In the following subsection, we discuss how the trajectory of the states and costates is affected by a change in the control and thus in this stored potential energy.

4.3.2.1. State Trajectory A change in the deflection-torque relation will in general change the force with which the link is pulled by the spring. In other words, it will influence the acceleration of the link $\ddot{x}_1$. The angular deflection x_1 and the link velocity, on the other hand, will not have an instantaneous change, since they are continuous physical quantities. Nevertheless, the normalized angular deflection we introduced in (25) will have a jump by the switching instants if the maximum angular deflection ϕ_{max} is changed. In order to simplify our discussion, we define the following new variables for the control, energy and the states as well as the maximum angular deflection along the switching structure:

$$\begin{aligned}
{}^iu &:= u \text{ after the } i-1\text{'th switch}\\
{}^iE &:= \text{Energy after the } i-1\text{'th switch}\\
{}^i\phi_{max} &:= \phi_{max} \text{ corresponding to } {}^iE\\
{}^ix_1 &:= x_1 \text{ after the } i-1\text{'th switch}\\
{}^i\dot{x}_1 &:= \dot{x}_1 \text{ after the } i-1\text{'th switch}\\
{}^ix_{10} &:= x_1 \text{ at the } i-1\text{'th switch}\\
{}^ix_1^* &:= x_1 \text{ at the } i\text{'th switch,}
\end{aligned}$$

with the corresponding normalized variables ${}^i\bar{x}_1 := \frac{{}^ix_1}{{}^i\phi_{max}}$, ${}^i\bar{x}_{10} := \frac{{}^ix_{10}}{{}^i\phi_{max}}$, ${}^i\bar{x}_1^* := \frac{{}^ix_1^*}{{}^i\phi_{max}}$ and $i \in \{1,2,\ldots\}$. The continuity of the displacement x_1 directly leads to a relation between ${}^i\bar{x}_1^*$ and ${}^{i+1}\bar{x}_{10}$:

$${}^ix_1^* = {}^{i+1}x_{10} \Rightarrow {}^{i+1}\bar{x}_{10} = {}^i\bar{x}_1^*\frac{{}^i\phi_{max}}{{}^{i+1}\phi_{max}}. \qquad (32)$$

Using (32), we see that $\bar{x}_1$ obviously never changes its sign after a switching. Furthermore, at the switching position ${}^ix_1^*$ a jump will always occur, unless the maximum displacements are equal to each other (${}^i\phi_{max} = {}^{i+1}\phi_{max}$) or the switching position is equal to zero (${}^i\bar{x}_1^* = 0$). We discuss now these jumps for different switching positions.

- **Switching at** $\bar{x}_1^* = 0$: According to (15), the control u can not change the energy E, when it changes the torque profile $\tau_{J,i}$ at $\bar{x}_1^* = 0$. On the other hand, the maximum displacement reachable with this energy depends on $\tau_{J,i}$ as can be observed from (17). In other words, if a switching occurs at $\bar{x}_1^* = 0$, ϕ_{max} will jump. Nevertheless, the jump in ϕ_{max} will not affect the normalized angular deflection $\bar{x}_1$, since x_1 is continuous, and we have ${}^i\bar{x}_1^* = {}^{i+1}\bar{x}_{10} = 0$.
- **Switching at** $\bar{x}_1^* \in (-1,1)\backslash\{0\}$: If the control u^* and thus the potential energy stored in the spring is increased, the maximum angular displacement that the link obtains by transforming all its kinetic energy into the potential energy decreases. Consequently, $|\bar{x}_1|$ will increase. Similarly, if u^* decreases, ϕ_{max} will increase and $|\bar{x}_1|$ will decrease instantaneously. Note that, no matter how the torque profiles look, ϕ_{max} will always remain positive and $|x_1| < \phi_{max}$ will hold, since the kinetic energy is positive. Consequently, we have $\bar{x}_{10} \in (-1,1)\backslash\{0\}$.
- **Switching at** $\bar{x}_1^* = \pm 1$: At the singularities, the link velocity is zero. Consequently ${}^i\phi_{max} = {}^{i+1}\phi_{max}$ holds and we have ${}^{i+1}\bar{x}_{10} = {}^i\bar{x}_1^* = \pm 1$.

4.3.2.2. Costate Trajectory As already mentioned, the analysis in Section 4.1, which led to analytical expressions for λ_2 and $\dot{\lambda}_2$, is valid only for a constant joint torque profile $\tau_J(\phi)$ with the corresponding constant energy E. At a switching position, this torque profile changes which in turn also changes this energy in general. Nevertheless, both these quantities remain constant until the next switching. In other words, the analytical expressions will remain valid between the switchings. Furthermore, the costates λ_2, $\dot{\lambda}_2$ are continuous along the whole trajectory including the switching instants. However, since the normalized deflection $\bar{x}_1^*$ at the switching positions is mostly not continuous as just discussed above, we can conclude that the boundary conditions λ_{20} and $\lambda_{20}^{'}$ in (26),(28) will in general jump at the switching positions. In order to distinguish between the costates corresponding to different switching times, the following additional variables are introduced for the costates:

$$\begin{aligned}
{}^i\lambda_2 &:= \lambda_2 \text{ after the } i-1\text{'th switch}\\
{}^i\lambda_2^{'} &:= \lambda_2^{'} \text{ after the } i-1\text{'th switch}\\
{}^ir &:= r \text{ after the } i-1\text{'th switch,}
\end{aligned}$$

with $i \in \{1, 2, \ldots\}$. Note that, the boundary conditions λ_{20} and $\lambda_{20}^{'}$ are not only influenced by a switching of u^*, but also when a singularity $\bar{x}_1 = \pm 1$ is reached (see Sec. 4.2 and Fig. 3) . Consequently, we will also need to sometimes distinguish between the costates before and after the singularity $\bar{x}_1 = \pm 1$ in our discussions. We discuss now the change of λ_{20}, $\lambda_{20}^{'}$ and r at the three different switching positions:

- **Switching at** $\bar{x}_1^* = 0$: From the continuity of λ_2 at $x_1^* = 0$ we have:
$$\lambda_2(0) = {}^{i}\lambda_{20} = {}^{i+1}\lambda_{20}. \tag{33}$$
Using our introduced notation we can also rewrite $\dot{\lambda}_2(0)$ as,
$$\dot{\lambda}_2(0) = {}^{i}\lambda_{20}^{'}\frac{{}^{i}\dot{x}_1(0)}{{}^{i}\phi_{max}} = {}^{i+1}\lambda_{20}^{'}\frac{{}^{i+1}\dot{x}_1(0)}{{}^{i+1}\phi_{max}}$$
$$\Rightarrow {}^{i+1}\lambda_{20}^{'} = \frac{{}^{i+1}\phi_{max}}{{}^{i}\phi_{max}}\ {}^{i}\lambda_{20}^{'}, \tag{34}$$
where we made use of the continuity of $\dot{\lambda}_2$ as well as $\dot{x}_1$. Using (33)-(34), we can then finally find how the ratio $r = \frac{\lambda_{20}}{\lambda_{20}^{'}}$ changes at $\bar{x}_1^* = 0$:
$${}^{i+1}r = \frac{{}^{i}\phi_{max}}{{}^{i+1}\phi_{max}}\ {}^{i}r. \tag{35}$$
- **Switching at** $\bar{x}_1^* \in (-1, 1)\backslash\{0\}$: According to (13), at a non-zero switching position $\lambda_2(\bar{x}_1^*)$ must be zero. Using again the continuity of λ_2, we can then conclude that
$${}^{i}\lambda_2({}^{i}\bar{x}_1^*) = {}^{i+1}\lambda_2({}^{i+1}\bar{x}_{10}) = 0, \tag{36}$$
where it is important to remember that after a switching at $\bar{x}_1 \neq 0$, a jump in $\bar{x}_1$ always occurs. Furthermore, from the condition (36), equation (31) and the fact that $I(\bar{x}_1)$ is a monotonously increasing, we can see that, $I({}^{i}\bar{x}_1^*) + {}^{i}r = 0$ must hold with a unique value of ${}^{i}\bar{x}_1^*$. In addition, since ${}^{i+1}\bar{x}_{10}$ lies in the interval $(-1, 1)$ as already discussed in Sec. 4.3.2.1, $I({}^{i+1}\bar{x}_{10}) + {}^{i+1}r = 0$ must hold as well and we have:
$${}^{i+1}r = -I({}^{i}\bar{x}_1^*\frac{{}^{i}\phi_{max}}{{}^{i+1}\phi_{max}}). \tag{37}$$
Evaluating $\dot{\lambda}_2(\bar{x}_1)$ in (28) at ${}^{i}\bar{x}_1^*$ and ${}^{i+1}\bar{x}_{10}$, we can then compute the change of the boudary condition $\lambda_{20}^{'}$ as:
$${}^{i+1}\lambda_{20}^{'} = \frac{{}^{i+1}\phi_{max}}{{}^{i}\phi_{max}}\frac{{}^{i}E}{{}^{i+1}E}\ {}^{i}\lambda_{20}^{'}. \tag{38}$$
Note that the change for the boundary condition λ_{20} can directly be computed using (37) and (38).
- **Switching at** $x_1^* = \pm 1$: Switchings will take place at the singularities only if $\lambda_2^*(\pm 1) = \frac{\mathrm{d}\lambda_2}{\mathrm{d}x_1}(0)\frac{2\ {}^{i}E}{{}^{i}\tau_J(\pm{}^{i}\phi_{max})} = 0$ holds, where ${}^{i}\tau_J := \tau_J(\phi, {}^{i}u)$. Since ${}^{i}E > 0$, we can furthermore see that this is only possible if ${}^{i}\lambda_{20}^{'}$ equals to zero. Noting that ϕ_{max} is not influenced at the switchings at $x_1^* = \pm 1$ and that λ_2 is continuous, we can than conclude:
$${}^{i+1}\lambda_{20}^{'} = {}^{i}\lambda_{20}^{'} = 0. \tag{39}$$
Evaluating $\dot{\lambda}_2$ at the singularities together with (39) yields then:
$${}^{i+1}\lambda_{20} = -\sqrt{\frac{{}^{i+1}E}{{}^{i}E}}\frac{{}^{i}\tau_J({}^{i}\phi_{max})}{{}^{i+1}\tau_J({}^{i}\phi_{max})}\ {}^{i}\lambda_{20}. \tag{40}$$
Note that, when there is a switching at $\bar{x}_1^* = \pm 1$, $\lambda_{20}^{'}$ always stays at zero according to (39) and r is undefined. Finally, since $\lambda_{20}^{'}$ does not change, the switching structure repeats itself (Switchings only at $\bar{x}_1 = 0$ and $\bar{x}_1 = \pm 1$).

Equations (32)-(40) provide all the equations needed to determine the change in the trajectory of the states and costates. Together with the analytical expressions (26)-(28) and the switching rule (31) illustrated graphically in Fig. 5, we have all the necessary tools to construct the optimal trajectory. Please note that for a given link mass M and given elastic torque boundaries $\tau_{J,1}, \tau_{J,2}$, the optimal switching positions are uniquely determined by the sign of $\lambda_{20}^{'}$ and the optimal initial ratio $r^*(0)$. Indeed, once an initial ratio is chosen, all the switching positions can be obtained by considering the direction of the link's movement, as well as the intersection points of the ratio r^* with the integral $I(\bar{x}_1)$, where the change of the ratio r^* at the maximum displacements $\bar{x}_1 = \pm 1$ as well as at the switching positions must be accounted for. These changes have been thoroughly discussed in Sections 4.2-4.3. In the following last subsection, we will show how to combine our results by investigating the optimal way to pump the maximum potential energy into two different VSA's.

4.4 Maximizing the Potential Energy of VSA's with adjustable linear and cubic springs

In this final section, we investigate the optimal way to change the elastic joint torque $\tau_J(\phi, u)$ of two VSA's, such that the stored potential energy in their springs is maximized at a given final time t_f. In particular, we examine one VSA with adjustable linear springs, $\tau_{J,i} = k_{l,i}\phi$ and one VSA with adjustable cubic springs, $\tau_{J,i} = k_{c,i}\phi^3 (i \in \{1, 2\})$, where both actuators start from the rest position with an initial link velocity [3] $(\phi = 0, \dot{\phi} > 0)$. Our main goal is to illustrate how to use the derived switching structure to solve such OC Problems and also to show how nonlinearities can affect the optimal strategy as well as the performance of VSA's.

Maximizing the potential energy in the springs is for both VSA's equivalent to maximizing the magnitude of the angular deflection $|\phi|$. Consequently, depending on the sign of the optimal deflection $\phi^*(t_f)$ the optimal strategy that maximizes the potential energy will minimize one of the two following cost functionals [4]: $J(u) = -x_1(t_f) \vee J(u) = x_1(t_f)$. According to (11), for both of these cost functionals the optimal costate $\lambda_2^*(t_f) = \frac{\partial\vartheta}{\partial x_2}$ is zero at the final time t_f. Consequently, if the ratio r^* is well-defined ($\lambda_{20}^{'} \neq 0$) trajectories that end exactly on the intersection point of r^* with $-I(\bar{x}_1)$ are candidates for the optimal trajectories that maximize the potential energy at this final time. Similarly, if $\lambda_{20}^{'} = 0$ and r^* is not defined, only trajectories that end at $\bar{x}_1^* = \pm 1$, where the link velocity is zero, can be optimal [5]. We have already discussed how choosing an initial sign for $\lambda_{20}^{'}$ together with an initial ratio $r(0)$ leads to a unique switching structure. Parameterizing $r(0) \in (-\infty, \infty)$ and noting that the switching structure for $\lambda_{20}^{'} = 0$ corresponds to the limiting case as $r(0) \to \pm\infty$, we can systematically compute for every given $\mathrm{sgn}(\lambda_{20}^{'})$ and $r(0)$ the switching

[3] We assume $\dot{\phi}$ to be initially positive without loss of generalization.
[4] The first cost functional is minimized if $\phi^*(t_f) > 0$ and the second functional if $\phi^*(t_f) < 0$.
[5] Note that if $\lambda_{20}^{'} = 0$, $\lambda_{20} \neq 0$ must hold. According to (26), λ_2 will then only be equal to zero when $\dot{x}_1 = 0$.

positions x_1^* at which $\lambda_2^*(x_1^*(t_f)) = 0$. The duration t_f needed to reach this position can simply be computed using the relation (18). The set of pairs $(t_f, x_1^*(t_f))$ found this way, will constitute of all solutions that satisfy the necessary conditions for optimality. Choosing among the solutions the ones that result in the maximum $|x_1^*(t_f)|$ yields the optimal strategy that maximizes the potential energy at t_f.

Figure 6 depicts the maximum deflection $\max|\phi(t_f)|$ for the two different VSA's mentioned above as a function of the final time t_f, where the figure is obtained following the procedure explained above ($k_{l,1} = 2\frac{Nm}{rad}$, $k_{l,2} = 8\frac{Nm}{rad}$, $k_{c,1} = 4\frac{Nm}{rad^3}$, $k_{c,2} = 16\frac{Nm}{rad^3}$, $M = 1\text{kgm}^2$, $\phi(0) = 0\text{rad}$, $\dot{\phi}(0) = 1\frac{rad}{s}$). Note that the parameters for the linear and cubic springs are chosen such that at $|\phi| = 1$ rad, the minimum and maximum storable potential energy in the springs are equal to each other ($\frac{1}{2}k_{l,i}^2 = \frac{1}{4}k_{c,i}^2, i \in \{1, 2\}$).

One important property regarding the optimal solution is that $\max|\phi(t_f)|$ is not a strictly increasing function of the final time. In other words, increasing t_f does not necessarily result to a higher potential energy at the final time. Secondly, having cubic springs is not really advantageous for our chosen parameters, if the final time is not high enough. Indeed, there is not a significant difference in the maximum displacements and consequently, only for final times t_f, where $\max|\phi(t_f)| > 1\text{rad}$, having cubic springs becomes beneficial. Nevertheless, for a sufficiently high t_f having nonlinearity in the springs can significantly increase the performance. For instance, for $t_f = 4\text{s}$, we see that the maximum potential energy stored in the linear spring is approximately 26.8J, whereas for the cubic spring this energy becomes 122J and thus more than four times higher.

Having discussed the optimal solution, we now want to compare the optimal switching structure for linear and nonlinear variable springs. Figure 7 depicts the trajectory of the optimal ratio r^* along the normalized deflection for $t_f = 2\text{s}$. The figure illustrates the change of r^* at the singularities and at the switching points but more importantly the way how the ratio r^* determines the switching points together with the integral $I(\bar{x}_1)$. A closer look at the switching structure for the linear spring (Fig. 7: Left) shows now that at the first two non-zero switching points the magnitude of the normalized deflection $|\bar{x}_1^*|$ does not change. This is due to the equivalence of the ratios $({}^3r = -{}^1r)$ and the symmetry of $I(\bar{x}_1)$. Actually, for any given initial ratio ${}^1r^*$, it can be shown that the magnitude of all the non-zero switching points $|\bar{x}_1^*|$ remain constant, even for larger final times t_f and that the ratio r^* keeps following the same trajectory along $\bar{x}_1$ (see the dotted line in Fig. 7: Left). Indeed, using (17), (35) and (37), we can show that at all the switching points including the switchings at $\bar{x}_1^* = 0$ we have:

$$ {}^{i+1}r = \sqrt{\frac{{}^{i+1}k_l}{{}^{i}k_l}}\ {}^{i}r, $$

where ${}^{i}k_l$ denotes the linear spring constant after the $i-1$' th switch. Since u^* is bang-bang along the optimal trajectory, we always have ${}^{i}k_l = {}^{i+2}k_l$ for all i. Furthermore, for linear springs Δ is equal to zero (see Table 1) and thus the ratio r^* only changes its sign at the singularities. Consequently, we can conclude from the symmetry of $I(\bar{x}_1)$ that $|{}^{i+2}r| = |{}^{i}r|$ holds for any $i \in \{1, 2, \ldots\}$. Note that changing at the same non-zero $|\bar{x}_1^*|$ implies that on the optimal trajectory, the ratio of the potential energy in the springs to the system's total energy remains always the same at the switchings. It is here worth noting that this same result was also found in Andresen et al. [2011] for a parametric oscillator, where the optimal control strategy maximizing the oscillator's energy is analysed. When we look now at the switching structure for the VSA with cubic springs, we can conclude that an intiutive switching structure similar to the VSA with linear springs does not exist. Indeed, since $\Delta \neq 0$ holds a symmetry in the switching positions does not exist and this makes the resulting structure more complex. Nevertheless, an initial choice for $r^*(0)$ uniquely determines all the switching positions as in the linear case.

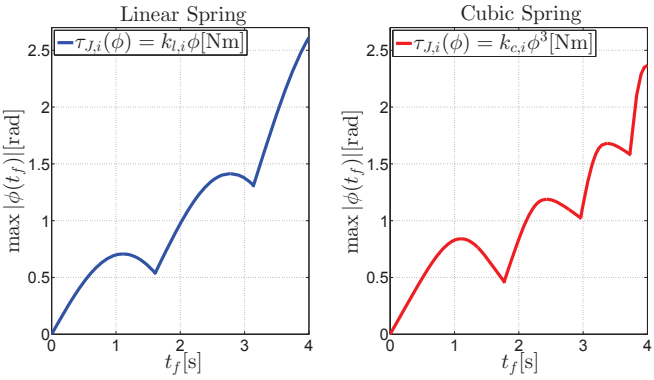

Fig. 6. Maximum Angular Deflection

5. CONCLUSION

In this paper, we presented a novel method to solve OC problems for VSA's, when a given terminal cost is to be minimized. The main advantages of the method are its direct relation to the system's physical quantities as well as its general applicability [6] . Since the solution provides us the best way to exploit the adjustable elasticity in joints, it can be used to analyse the maximum performance we can gain from these actuators as we have illustrated in Section 4.4 for VSA's with linear and cubic springs.

Clearly, there are still open questions regarding the optimal control of elastic joints, especially for systems with multiple joints. We see the description of optimal control strategies in terms of physical quantities as the key to understanding these systems. Our current research focuses on extending the introduced method for systems with multiple degrees of freedom and also to analysing the influence of the dynamics of the VSA on the optimal control strategy.

6. ACKNOWLEDGMENT

This work has been partially funded by the European Commissions Sixth Framework Programme as part of the project SAPHARI under grant no. 287513.

Appendix A. THE INTEGRAL I

In this Appendix, we will show that the integral $I(\bar{x}_1)$ diverges at $\bar{x}_1 = \pm 1$. Since, $I(\bar{x}_1)$ is symmetrical with respect to the origin, it is sufficient to show that the improper integral $I(1)$ is divergent. Using the substitution

[6] Note that we only assume to have a strictly increasing continuously differentiable deflection-torque relation, which is satisfied in most existing designs.

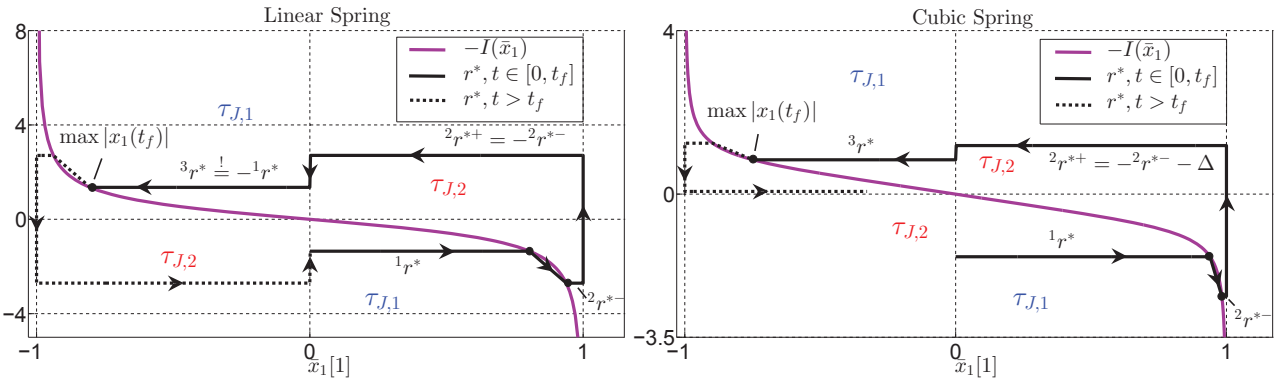

Fig. 7. Optimal Ratio r^* along the Optimal Trajectory (Left: Linear Spring, Right: Cubic Spring)

$y(\bar{x}_1) = \frac{\dot{\phi}^2_{max} - \dot{x}^2_1(\bar{x}_1)}{\dot{\phi}^2_{max}} = \frac{\int_0^{\bar{x}_1 x_{1max}} \tau_J(\phi)\mathrm{d}\phi}{E}$, we can rewrite $I(\bar{x}_1)$ as:

$$I(\bar{x}_1) = \frac{E}{\phi_{max}} \int_{y(0)=0}^{y(\bar{x}_1)} \left(\frac{1}{1-y}\right)^{\frac{3}{2}} \frac{\mathrm{d}y}{\tau_J(x_1(y))},$$

where we note that at $y = 0$, the integrand is now not defined, as well. Noting that τ_J is strictly increasing and positive in $\bar{x}_1 \in (0, 1]$, we have for any positive scalar ε less than 1:

$$\begin{aligned} I(1) &> \frac{E}{\phi_{max}} \int_{\varepsilon}^{1} \left(\frac{1}{1-y}\right)^{\frac{3}{2}} \frac{\mathrm{d}y}{\tau_J(x_1(y))} \\ &> \frac{E}{\phi_{max}\tau_J(\phi_{max})} \int_{\varepsilon}^{1} \frac{1}{1-y}. \end{aligned}$$

The integral $\int_{\varepsilon}^{1} \frac{1}{1-y} = \ln(1-\varepsilon) - \lim_{y\to 1}(1-y) = \infty$ diverges. According to Comparison Test (Rudin [1976]), we can then conclude that I is always divergent at the singular points $\bar{x}_1 = \pm 1$.

REFERENCES

M. Abramowitz and I.A. Stegun. *Handbook of Mathematical Functions: With Formulas, Graphs, and Mathematical Tables*. Applied mathematics series. Dover Publications, 1964.

B Andresen, K H Hoffmann, J Nulton, A Tsirlin, and P Salamon. Optimal control of the parametric oscillator. *European Journal of Physics*, 32(3):827, 2011.

A. Bicchi and G. Tonietti. Fast and soft arm tactics: Dealing with the safety-performance trade-off in robot arms design and control. *IEEE Robotics and Automation Mag.*, 11:22–33, 2004.

D. Braun, M. Howard, and S. Vijayakumar. Exploiting variable stiffness in explosive movement tasks. In *Proceedings of Robotics: Science and Systems (RSS2011), Los Angeles, USA*, June 2011.

M. Braun. *Differential Equations and Their Applications: An Introduction to Applied Mathematics*. Texts in Applied Mathematics. Springer, 1993.

O. Eiberger, S. Haddadin, M. Weis, A. Albu-Schäffer, and G. Hirzinger. On joint design with intrinsic variable compliance: Derivation of the DLR QA-joint. *IEEE Int. Conf. on Robotics and Automation (ICRA2010), Anchorage, Alaska*, pages 1687–1694, 2010.

M. Garabini, A. Passaglia, F. A. W. Belo, P. Salaris, and A. Bicchi. Optimality principles in variable stiffness control: the vsa hammer. *2011 IEEE/RSJ International Conference on Intelligent Robots and Systems (IROS2011), San Francisco, USA*, pages 3770 – 3775, 2011.

S. Haddadin, F. Huber, and A. Albu-Schäffer. Optimal control for exploiting the natural dynamics of variable stiffness robots. In *Robotics and Automation (ICRA), 2012 IEEE International Conference on*, pages 3347–3354, 2012a.

S. Haddadin, M. C. Özparpucu, and A. Albu-Schäffer. Optimal control for maximizing potential energy in a variable stiffness joint. In *Decision and Control (CDC), 2012 IEEE 51st Annual Conference on*, pages 1199–1206, 2012b.

Jun Nakanishi and Sethu Vijayakumar. Exploiting passive dynamics with variable stiffness actuation in robot brachiation. In *Robotics: Science and Systems*, 2012.

A.H. Nayfeh and D.T. Mook. *Nonlinear Oscillations*. Wiley, 1995.

M. Papageorgiou. *Optimierung: Statische, dynamische, stochastische Verfahren*. Oldenbourg, 1996.

G.A. Pratt and M.M. Williamson. Series elastic actuators. In *Intelligent Robots and Systems 95. 'Human Robot Interaction and Cooperative Robots', Proceedings. 1995 IEEE/RSJ International Conference on*, volume 1, pages 399–406 vol.1, 1995.

W. Rudin. *Principles of Mathematical Analysis*. International series in pure and applied mathematics. McGraw-Hill International, 1976.

L.F. Shampine. Vectorized adaptive quadrature in matlab. *Journal of Computational and Applied Mathematics*, 211(2):131 – 140, 2008.

Ronald van Ham, Thomas Sugar, Bram Vanderborgth, Kevin Hollander, and Dirk Lefeber. Compliant actuator designs: Review of actuators with passive adjustable compliance/controllable stiffness for robotic applications. *IEEE Robotics and Automation Mag.*, 16(3): 81–94, 2009.

S. Wolf and G. Hirzinger. A new variable stiffness design: Matching requirements of the next robot generation. *IEEE Int. Conf. on Robotics and Automation (ICRA 2008), Pasadena, USA*, pages 1741–1746, 2008.

S. Wolf, O. Eiberger, and G. Hirzinger. The dlr fsj: Energy based design of a variable stiffness joint. In *Robotics and Automation (ICRA)*, pages 5082–5089, 2011.